Experimental Determination of Irreversible Entropy Production in out-of-Equilibrium Mesoscopic Quantum Systems

Citation for the original published paper (version of record):
Brunelli, M., Fusco, L., Landig, R. et al (2018). Experimental Determination of Irreversible Entropy Production in out-of-Equilibrium Mesoscopic
Quantum Systems. Physical Review Letters, 121(16).
http://dx.doi.org/10.1103/PhysRevLett.121.160604

Editors' Suggestion | Featured in Physics

Experimental Determination of Irreversible Entropy Production in out-of-Equilibrium Mesoscopic Quantum Systems

M. Brunelli,[1] L. Fusco,[2] R. Landig,[3,*] W. Wieczorek,[4] J. Hoelscher-Obermaier,[5,6] G. Landi,[7] F. L. Semião,[8] A. Ferraro,[2] N. Kiesel,[5] T. Donner,[3] G. De Chiara,[2] and M. Paternostro[2]

[1]*Cavendish Laboratory, University of Cambridge, Cambridge CB3 0HE, United Kingdom*

[2]*Centre for Theoretical Atomic, Molecular and Optical Physics, School of Mathematics and Physics, Queen's University, Belfast BT7 1NN, United Kingdom*

[3]*Institute for Quantum Electronics, ETH Zürich, 8093 Zürich, Switzerland*

[4]*Department of Microtechnology and Nanoscience, Chalmers University of Technology, 412 96 Göteborg, Sweden*

[5]*University of Vienna, Faculty of Physics, Vienna Center for Quantum Science and Technology (VCQ), Boltzmanngasse 5, 1090 Vienna, Austria*

[6]*Leibniz University Hannover, Institute for Gravitational Physics (Albert-Einstein-Institute), Callinstraße 38, 30167 Hannover, Germany*

[7]*Instituto de Física da Universidade de São Paulo, 05314-970 São Paulo, Brazil*

[8]*Centro de Ciências Naturais e Humanas, Universidade Federal do ABC, 09210-170 Santo André, São Paulo, Brazil*

(Received 3 July 2018; published 17 October 2018)

By making use of a recently proposed framework for the inference of thermodynamic irreversibility in bosonic quantum systems, we experimentally measure and characterize the entropy production rates in the nonequilibrium steady state of two different physical systems—a micromechanical resonator and a Bose-Einstein condensate—each coupled to a high finesse cavity and hence also subject to optical loss. Key features of our setups, such as the cooling of the mechanical resonator and signatures of a structural quantum phase transition in the condensate, are reflected in the entropy production rates. Our work demonstrates the possibility to explore irreversibility in driven mesoscopic quantum systems and paves the way to a systematic experimental assessment of entropy production beyond the microscopic limit.

DOI: 10.1103/PhysRevLett.121.160604

Entropy is a crucial quantity for the characterization of dynamical processes: it quantifies and links seemingly distant notions such as disorder, information, and irreversibility across different disciplinary boundaries [1,2]. Every finite-time transformation results in some production of entropy, which signals the occurrence of irreversibility. Quantifying the amount of irreversible entropy produced by a given process is a goal of paramount importance: *entropy production* is a key quantity for the characterization of nonequilibrium processes, and its minimization improves the efficiency of thermal machines. The second law of thermodynamics can be formulated in terms of a universal constraint on the entropy production, which can never be negative [3,4]. In turn, this leads to the following rate equation for the variation of the entropy S [5]:

$$\frac{dS}{dt} = \Pi(t) - \Phi(t), \tag{1}$$

where $\Pi(t)$ and $\Phi(t)$ are the irreversible entropy production rate and the entropy flux from the system to the environment, respectively. When the system reaches a nonequilibrium steady state (NESS), these quantities take values Π_s and Φ_s respectively, such that $\Pi_s = \Phi_s > 0$ [see Fig. 1(a)]. Under these conditions, entropy is produced and exchanged with the local baths at the same rate. Only when both terms vanish ($\Pi_s = \Phi_s = 0$) does one recover thermal equilibrium. The entropy production rate directly accounts for the irreversibility of a process and uncovers the nonequilibrium features of a system.

The link between the entropy production rate Π_s and irreversibility becomes particularly relevant in small systems subjected to fluctuations for which a microscopic definition of entropy production based on stochastic trajectories of the system has been given [6]. Experimentally, this notion has been used to test fluctuation theorems in a variety of classically operating systems such as a single-electron box [7], a two-level system driven by a time-dependent potential [8], and a levitated nanoparticle undergoing relaxation [9]. However, in order to harness the working principles of thermodynamic machines working at the quantum level, and pinpoint the differences between their performances and those of their classical counterparts, it is important to analyze the entropy generated through genuine quantum dynamics [10]. Moreover, while so far nanoscale systems have been used for the experimental study of classical out-of-equilibrium thermodynamics, irreversible entropy production arising from quantum

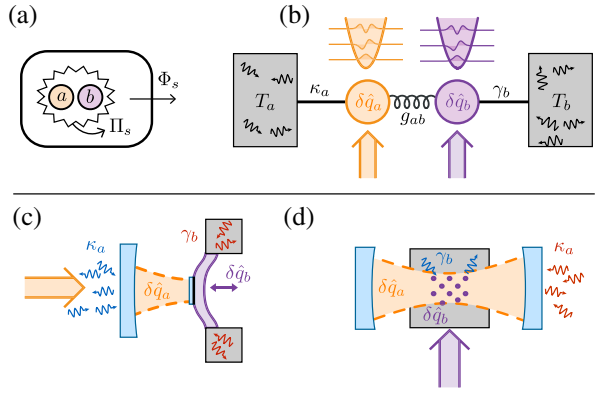

FIG. 1. (a) The driven-dissipative system, consisting of the coupled subsystems a and b, reaches a nonequilibrium steady state (NESS) with an associated entropy production rate Π_s and an entropy flux Φ_s from the system to the environment. (b) The systems can be modelled as two quantum harmonic oscillators at frequencies ω_a and ω_b, linearly coupled with a strength g_{ab}. Each oscillator is coupled to independent local baths at temperature T_a and T_b, respectively. The corresponding coupling rates are κ_a and γ_b. The oscillators can be pumped by an external field (purple and orange arrows in the figure). (c) Optomechanical setup: a micromechanical oscillator ($\delta\hat{q}_b$) is coupled to the field mode of an optical Fabry-Perot cavity ($\delta\hat{q}_a$). For this setup only the cavity is pumped. (d) Cavity-BEC setup: the external degree of freedom of a BEC ($\delta\hat{q}_b$) is coupled to the field mode of a cavity ($\delta\hat{q}_a$). For this setup only the atoms are pumped. Red and blue wiggly lines indicate heating or cooling of the subsystems via coupling to the baths. In both setups the number of excitations in the optical bath is zero, i.e., $n_{T_a} = 0$.

dynamics in mesoscopic quantum systems has not been experimentally investigated yet.

Recently, progress towards the theoretical characterization of entropy production in bosonic systems brought out of equilibrium has been made [11–13]. In this Letter, we make use of such theoretical framework to quantify experimentally the amount of irreversibility in the NESS of two different driven-dissipative quantum systems, realized by coupling bosonic systems to high-finesse cavities. The light field mode of a cavity allows us to infer the entropy production in terms of relevant controllable parameters of the coupled system. In particular, in this study, we investigate the influence of different dynamical regimes and sources of environmental noise on the quantum fluctuations of a quantum system, and thus the corresponding entropy production rate. In order to address such influences, we assess two distinct experimental setups: a cavity-optomechanical (cavity-OM) device and a Bose-Einstein condensate (BEC) with cavity-mediated long-range interactions [14–16]. The required measurements are based on the spectra of the light fields leaking out of the respective cavities. Remarkably, the entropy production reflects the specific features of the two experimental platforms, which are very different in nature despite the common description provided here. As such, our results show how a key indicator of irreversibility is fully within the grasp of dynamically controlled quantum dynamics.

In cavity-OM systems, the cavity photon number is coupled to the position of the mechanical oscillator [cf. Figs. 1(b) and 1(c)]. Our specific implementation uses a Fabry-Perot cavity. One of its mirrors is a doubly clamped, highly reflective, mechanical cantilever. Radiation pressure couples the intracavity photon number to the position of the cantilever. The mechanical support of the cantilever provides a local heat bath at room temperature. The optical cavity is driven by a laser that is red detuned by the mechanical frequency from the optical cavity resonance. For a driving laser without classical noise, the cavity mode is coupled to a zero-excitation heat bath. We observe sideband cooling of the mechanical motion [17–20] and, for large drive powers, strong optomechanical coupling [21–23]. To analyze the entropy production rate of the cavity-OM system, we measure the light reflected off the cavity via homodyne detection.

Also in the second implementation, the two coupled harmonic oscillators correspond to a light field mode coupled to a mechanical degree of freedom [cf. Figs. 1(b) and 1(d)]. We load a BEC into a high-finesse optical cavity and illuminate the atoms with a standing-wave transverse laser field. Far-off resonant scattering of photons from the laser field into a near-detuned, initially empty cavity field mode, couples the zero-momentum mode of the BEC to an excited momentum mode. The scattering process mediates effective atom-atom interactions, which are long range, since the photons are delocalized in the cavity mode [16]. This interaction is tunable in strength via the power of the transverse laser beam. The long-range interaction can be brought to competition with the kinetic energy of the atoms, resulting in a structural phase transition [24]. In the spatially homogeneous phase, for increasing interaction, the energy of the excited momentum mode softens until, at a critical interaction, the strength of the system breaks a discrete symmetry and the atoms arrange in a spatially modulated density distribution. The equivalence of this system to a Dicke model has been demonstrated in Ref. [15]. We measure the cavity light field leaking through the mirrors with a heterodyne detection setup. The spectral analysis of this signal is used to infer the diverging amount of atomic density fluctuations accompanying the structural phase transition [24].

In both cases, the effective interaction between the oscillators is obtained by a harmonic expansion of the field operators around their mean values, resulting in two linearly coupled quantum oscillators [cf. Fig. 1(b)]. We denote with $\delta\hat{q}_{a,b}$ and $\delta\hat{p}_{a,b}$ the position and momentum fluctuation operators around the mean-field values of the two oscillators. In what follows, a and b refer to the optical and mechanical or atomic oscillators, respectively. In a frame rotating at the frequency ω_p of the respective pump

fields, the oscillators have frequencies $\omega_a = \omega_c - \omega_p$ and ω_b (here ω_c is the frequency of the cavity field). Their interaction is described by the Hamiltonian

$$\hat{H} = \frac{\hbar\omega_a}{2}(\delta\hat{q}_a^2 + \delta\hat{p}_a^2) + \frac{\hbar\omega_b}{2}(\delta\hat{q}_b^2 + \delta\hat{p}_b^2) + \hbar g_{ab}\delta\hat{q}_a\delta\hat{q}_b, \tag{2}$$

where g_{ab} is the coupling strength between the modes. In the superradiant phase of the Dicke model, an additional squeezing term of the atomic mode must be included in the Hamiltonian [16]. For the derivation of the models and the values of the parameters in the two setups, we refer to Ref. [25] and to Table I. The systems are inherently open: each harmonic oscillator is independently coupled to a local bath. This provides both a dissipation channel and extra quantum fluctuations in addition to those present in the closed systems. The optical cavity mode is coupled to the surrounding electromagnetic vacuum with a decay rate κ_a. On the other hand, the nature of the mechanical or atomic bath is specific to the setup being considered. In the cavity-OM system, the coupling of the vibrating mirror to the background of phonon modes is described in terms of quantum Brownian motion. In the cavity-BEC system, dissipation is due to the collection of excited Bogolioubov modes, which provides a bath for the condensate. In both cases, we assume oscillator b to be in contact with a Markovian bath at temperature T_b and rate γ_b. The average number of excitations in the equilibrium state of oscillator b is thus $n_{T_b} = (e^{\hbar\omega_b/k_B T_b} - 1)^{-1}$ (cf. Ref [31]). The driven-dissipative nature of the systems is such that a NESS is eventually reached [14,32].

The linear dynamics undergone by the coupled oscillators allows us to exploit a framework developed for linear stochastic processes [11–13]. In particular, the situation that we face is perfectly suited to the use of the framework for the quantification of entropy production proposed in Ref. [12], where the entropy S of an arbitrary bosonic quantum system prepared in a Gaussian state is written in terms of the Shannon entropy of the Wigner function

$$S(t) = -\int \mathcal{W}(u,t)\log\mathcal{W}(u,t)du, \tag{3}$$

where $\mathcal{W}(u,t)$ is the Wigner function at time t corresponding to the state of the two oscillators, and u is the corresponding vector of complex phase-space variables. The quadratic nature of Eq. (2) and the initial thermal state of the oscillators in both setups ensures the positivity of $\mathcal{W}(u,t)$ and allows us to write it in terms of the variances of the fluctuation operators of the oscillators, which enormously simplifies the explicit calculation of $\Pi(t)$. In the NESS, all entropy produced in the system flows to the environments so that $\Pi_s = \Phi_s$. Following the lines sketched in Ref. [25], the entropy production rate in the NESS due to the quantum fluctuations takes the form

$$\Pi_s = \Phi_s = 2\gamma_b\left(\frac{n_b + 1/2}{n_{T_b} + 1/2} - 1\right) + 4\kappa_a n_a = \mu_b + \mu_a, \tag{4}$$

where $n_a = \langle(\delta\hat{q}_a^2 + \delta\hat{p}_a^2 - 1)\rangle_s/2$ and $n_b = \langle(\delta\hat{q}_b^2 + \delta\hat{p}_b^2 - 1)\rangle_s/2$ are the average number of excitations in the NESS of the two oscillators in excess of the zero-point motion of the respective harmonic oscillator. In the cavity-OM expression for μ_b, instead of the full phonon number n_b, only the momentum variance $\langle\delta\hat{p}_b^2\rangle_s$ enters as we assume Brownian motion damping.

Equation (4) represents our main theoretical result: it quantifies the entropic contribution, ascribable to the quantum fluctuations that the system has to pay to remain in its NESS. It thus directly quantifies the irreversibility of the driven-dissipative dynamics of two linearly coupled quantum oscillators, well beyond the linear-response limit. For vanishing coupling, the systems reach thermal equilibrium (i.e., $n_a = 0$ and $n_b = n_{T_b}$), and Π_s vanishes. Moreover, there is no dependence on the correlations between the oscillators, since in a NESS the entropy production rate Π_s equals the flux rate Φ_s. Thus, the entropy flux from the system to the overall environment determines the amount of *irreversibility* produced within the driven-dissipative model, and is directly linked to the breaking down of the microscopic detailed balance [10]. The previous considerations also allow us to identify two contributions to Π_s, linked to the mechanical or atomic and optical oscillator, referred to as μ_a and μ_b, respectively. They are the individual entropy flows to each environment and show how the entropy produced in the NESS is split into two distinct fluxes. We note that the explicit form of Eq. (4) in terms of the sum of such independent terms strongly relies on the local nature of the environments that we have considered, and we expect it not to hold in more general situations. The dissipative evolution arising from

TABLE I. Physical parameters for the two experimental setups. The damping rate γ_b is constant in the cavity-OM experiment, while in the cavity-BEC setup it depends on the actual working point (cf. Ref. [25] for details). Here, m is the effective mass of the mechanical oscillator, and N is the number of ^{87}Rb atoms in the BEC.

	$\omega_a/2\pi$ [MHz]	$\kappa_a/2\pi$ [kHz]	$\omega_b/2\pi$ [kHz]	$\gamma_b/2\pi$ [Hz]	T_b [K]	Other parameters
cavity-OM	1.27815	435.849	1278.15	264.1	292	$m = 176$ ng
cavity-BEC	15.13	1250	8.3	[25]	38×10^{-9}	$N = 10^5$

the contact with the environments is manifested explicitly in Eq. (4) by the presence of the rates γ_b and κ_a. In both settings, the mechanical or atomic damping rate γ_b is much smaller than the cavity decay rate κ_a, as can be appreciated from Table I.

A general formulation of entropy production demands the knowledge of the global state of the system [33–37]. However, Π_s evaluated for the linearized dynamics in Eq. (2) only involves the mean excitations of the oscillators [11,13]. For the experimental regime of interest, the dynamics of the cavity field adiabatically follows the mechanical or atomic mode. By measuring the light field leaking out of the cavity, we thus can infer about both μ_a and μ_b. For both experimental setups, the coupling g_{ab} is varied by increasing the power of the pump. The density noise spectrum (DNS) of the cavity field quadratures is recorded [24,38]. Typical examples of the experimental DNS, together with the fitting curves used for their analysis, are shown in Fig. 2. In the cavity-OM experiment, the data sets are taken for $\omega_a = \omega_b$, which is the working point where the cooling of the mechanical resonator is most effective in the resolved-sideband regime. In the cavity-BEC experiment, on the other hand, the parameters are $\omega_a \gg \omega_b$, resulting in only a tiny admixture of the optical subsystem. A further difference between the two platforms is in the way the two oscillators are populated: in the optomechanical case, we have $n_b \gg n_a$ for the lowest coupling values, while they become comparable in size for the maximum cooling achieved. In the cavity-BEC setup, the cavity field is considerably less populated than the atomic mode. Finally, the mechanical bath is at room temperature, while the temperature of the atomic reservoir is below the condensation point and in the nK range (cf. Table I). This highlights and reinforces the diversity of the experimental platforms that we have addressed within a unique framework for the quantification of irreversible entropy.

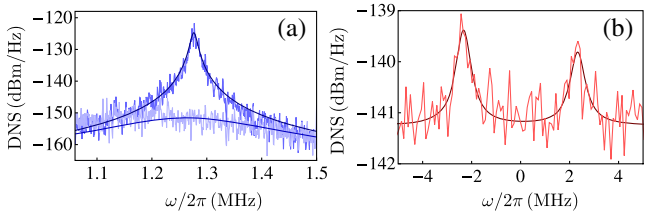

FIG. 2. Experimental density noise spectra. Panel (a): Density noise spectrum (DNS) of the phase quadrature of the output cavity field, attenuated before detection, for the cavity-OM setup. The jagged blue curve refers to a value of the rescaled coupling $g_{ab}/\kappa_a = 0.49$, while the jagged light-blue curve to $g_{ab}/\kappa_a = 2.29$. The fits of the DNS are shown as smooth lines. Notice that the power spectrum is originally dimensionless, and has been here converted to SI units for uniformity of notation. Panel (b): DNS of the extra-cavity field for the cavity-BEC system at a coupling $(g_{ab}/g_{ab}^{\mathrm{cr}})^2 = 0.93$. A fit of the DNS is shown as a smooth line.

Following the technical approach illustrated in Refs. [11–13] and sketched in [25], we have separately reconstructed the two terms μ_a and μ_b that determine quantitatively Π_s. Figure 3 displays the experimental data together with the theoretical model, demonstrating a very good quantitative agreement. Besides the influences of the environments, the entropy production rates depend on the interplay between the *mutual dynamics* of the oscillators. For the cavity-OM system, the contribution to Π_s we

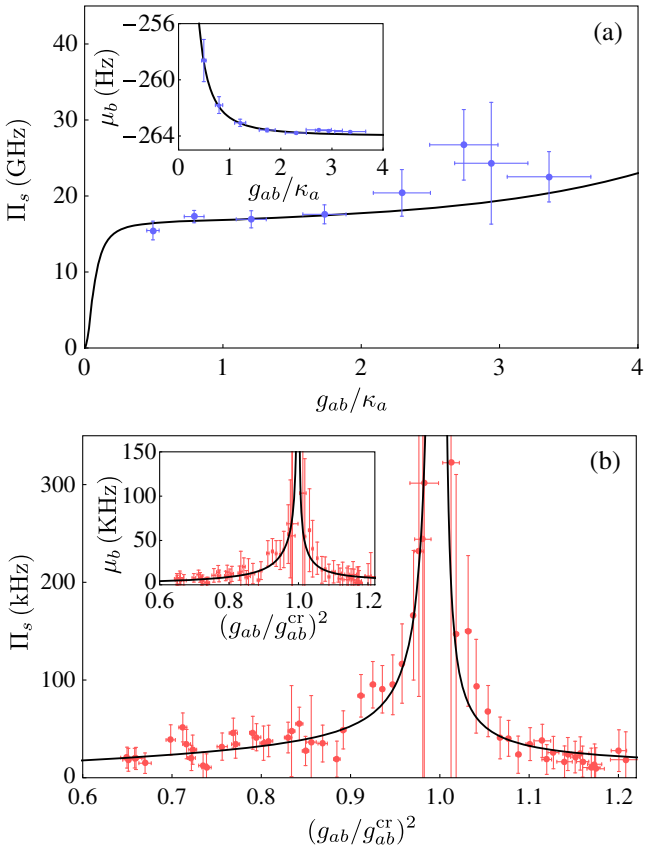

FIG. 3. Experimental assessment of the irreversible entropy production rate Π_s at the NESS for (a) the cavity-OM system and (b) the cavity-BEC system. In the cavity-OM system, g_{ab} is twice the standard optomechanical coupling rate [14,25]. For the cavity-BEC setup, the control parameter g_{ab} is renormalized with respect to the critical parameter $g_{ab}^{\mathrm{cr}} = \sqrt{(\kappa_a^2 + \omega_a^2)\omega_b/4\omega_a}$. The insets show the behavior of μ_b in each of the settings considered. In both panels, the solid black lines show the theoretical predictions based on the values given in Table I. The blue and red dots show the experimental data for the cavity-OM and cavity-BEC experiment, respectively. In panel (a), the vertical error bars report statistical errors extracted from the fit, while the horizontal ones show experimental error on the values of the parameter. In panel (b), the vertical and horizontal error bars report the statistical errors from the fit and the determination of the critical point, respectively [24].

observe from the mechanical oscillator is much smaller than the one coming from the optical field. On the contrary, $\mu_a \simeq \mu_b$ in the atomic setup. For each of the two experiments Π_s is positive, in agreement with the second law. In the cavity-OM setup, μ_a is an increasing function of the coupling: the stronger the pump, the further the system operates away from thermal equilibrium and the more entropy is generated. At the same time, μ_b takes negative values, whose magnitude increases for increasing values of g_{ab}. This is legitimate as μ_b is not *per se* an entropy production rate, but represents an individual flux, which can thus take negative values (while $\mu_a + \mu_b$ has to be positive). The observed behavior of μ_b is a signature of optomechanical cooling: its growth, in absolute value, with g_{ab} shows the increase of the entropy flow from the mechanical resonator to the cavity field, corresponding to lowering of the effective temperature of the resonator. As for the cavity-BEC system, the divergent behavior of the entropy production rate at the critical point reflects the occurrence of the structural phase transition: at g_{ab}^{cr}, the known divergence of the populations of the two oscillators at the steady state [39] results in the singularity of both μ_a and μ_b separately. The irreversible entropy production rate thus diverges at criticality.

We have experimentally determined the entropy production rate, a key indicator of irreversibility, in driven-dissipative quantum systems operating at the steady state. The two experimental setups, being instances of mesoscopic systems undergoing quantum dynamics, allowed us to link the phenomenology of the entropy production rate to the salient features of their physics. We have thus assessed architectures that could embody the building blocks of a generation of future thermodynamic machines working out of equilibrium, and thus subjected to irreversible processes. For such devices, the quantification of irreversibility will be very relevant for the characterization of their efficiency, as it will provide useful information to design protocols able to quench it, thus optimizing their working principles.

We are grateful to M. Aspelmeyer, T. Esslinger, J. Goold, I. Lesanovsky, E. Lutz, and J. Schmiedmayer for useful comments and fruitful discussions during the development of this project. We thank S. Gröblacher for support with microfabrication, and F. Brennecke and R. Mottl for support in taking and evaluating the cavity-BEC data. This work was supported by the European Union through the projects TherMiQ, TEQ, SIQS, iQOEMS, and ITN cQOM, the European Research Council through the Advanced Grant project SQMBS, the Brazilian CNPq through Grant No. 302900/2017-9 and the "Ciência sem Fronteiras" program via the "Pesquisador Visitante Especial" initiative (Grant No. 401265/2012-9), the São Paulo Research Foundation (FAPESP) under Grant No. 2014/01218-2, the Brazilian National Institute of Science and Technology of Quantum Information (INCT/IQ), the Vienna Science and Technology Fund (WWTF, Project No. ICT12-049), and the Austrian Science Fund FWF (JHO: W1210, CoQuS; NK: AY0095221, START).

*Present address: Department of Physics, Harvard University, Cambridge, Massachusetts 02138, USA.

[1] J. P. Sethna, *Entropy, Order Parameters, and Complexity* (Oxford University Press, Oxford, 2011).
[2] M. W. Zemansky, *Heat and Thermodynamics* (McGraw-Hill Book Company Inc., New York, 1968).
[3] U. Seifert, Rep. Prog. Phys. **75**, 126001 (2012).
[4] C. Jarzynski, Annu. Rev. Condens. Matter Phys. **2**, 329 (2011).
[5] R. C. Tolman and P. C. Fine, Rev. Mod. Phys. **20**, 51 (1948).
[6] U. Seifert, Phys. Rev. Lett. **95**, 040602 (2005).
[7] J. V. Koski, T. Sagawa, O-P. Saira, Y. Yoon, A. Kutvonen, P. Solinas, M. Möttönen, T. Ala-Nissila, and J. P. Pekola, Nat. Phys. **9**, 644 (2013).
[8] C. Tietz, S. Schuler, T. Speck, U. Seifert, and J. Wrachtrup, Phys. Rev. Lett. **97**, 050602 (2006).
[9] J. Gieseler, R. Quidant, C. Dellago, and L. Novotny, Nat. Nanotechnol. **9**, 358 (2014).
[10] T. B. Batalhão, A. M. Souza, R. S. Sarthour, I. S. Oliveira, M. Paternostro, E. Lutz, and R. M. Serra, Phys. Rev. Lett. **115**, 190601 (2015).
[11] G. T. Landi, T. Tomé, and M. J. de Oliveira, J. Phys. A **46**, 395001 (2013).
[12] J. P. Santos, G. Landi, and M. Paternostro, Phys. Rev. Lett. **118**, 220601 (2017).
[13] M. Brunelli and M. Paternostro, arXiv:1610.01172.
[14] M. Aspelmeyer, T. Kippenberg, and F. Marquardt, Rev. Mod. Phys. **86**, 1391 (2014).
[15] K. Baumann, C. Guerlin, F. Brennecke, and T. Esslinger, Nature (London) **464**, 1301 (2010).
[16] R. Mottl, F. Brennecke, K. Baumann, R. Landig, T. Donner, and T. Esslinger, Science **336**, 1570 (2012).
[17] A. Schliesser, R. Rivière, G. Anetsberger, O. Arcizet, and T. Kippenberg, Nat. Phys. **4**, 415 (2008).
[18] S. Gröblacher, J. B. Hertzberg, M. R. Vanner, G. D. Cole, S. Gigan, K. C. Schwab, and M. Aspelmeyer, Nat. Phys. **5**, 485 (2009).
[19] J. Chan, T. P. Mayer Alegre, A. H. Safavi-Naeini, J. T. Hill, A. Krause, S. Gröblacher, M. Aspelmeyer, and O. Painter, Nature (London) **478**, 89 (2011).
[20] J. D. Teufel, T. Donner, D. Li, J. W. Harlow, M. S. Allman, K. Cicak, A. J. Sirois, J. D. Whittaker, K. W. Lehnert, and R. W. Simmonds, Nature (London) **475**, 359 (2011).
[21] S. Gröblacher, K. Hammerer, M. R. Vanner, and M. Aspelmeyer, Nature (London) **460**, 724 (2009).
[22] E. Verhagen, S. Deléglise, S. Weis, A. Schliesser, and T. J. Kippenberg, Nature (London) **482**, 63 (2012).
[23] J. D. Teufel, Dale Li, M. S. Allman, K. Cicak, A. J. Sirois, J. D. Whittaker, and R. W. Simmonds, Nature (London) **471**, 204 (2011).
[24] R. Landig, F. Brennecke, R. Mottl, T. Donner, and T. Esslinger, Nat. Commun. **6**, 7046 (2015).

[25] See Supplementary Material accompanying this manuscript, and available from http://link.aps.org/supplemental/10.1103/PhysRevLett.121.160604, where additional details on the formal derivation of the rate of entropy production and experimental methods are illustrated, and which includes Refs. [26–30].
[26] G. Adesso, D. Girolami, and A. Serafini, Phys. Rev. Lett. **109**, 190502 (2012).
[27] V. Giovannetti and D. Vitali, Phys. Rev. A **63**, 023812 (2001).
[28] A. A. Clerk, M. H. Devoret, S. M. Girvin, F. Marquardt, and R. J. Schoelkopf, Rev. Mod. Phys. **82**, 1155 (2010).
[29] R. H. Dicke, Phys. Rev. **93**, 99 (1954).
[30] W. Kopylov, C. Emary, and T. Brandes, Phys. Rev. A **87**, 043840 (2013).
[31] The observed atomic damping, for the cavity-BEC setup, takes place on time scales longer than the time scale of the appearance of polariton modes. Thus the Bose distribution function, for the thermal number of excitation, is evaluated at the softening frequency of the atomic polariton mode (see Supplemental Material).
[32] F. Brennecke, R. Mottl, K. Baumann, R. Landig, T. Donner, and T. Esslinger, Proc. Natl. Acad. Sci. U.S.A. **110**, 11763 (2013).
[33] R. E. Spinney and I. J. Ford, Phys. Rev. E **85**, 051113 (2012).
[34] G. Crooks, Phys. Rev. E **61**, 2361 (2000).
[35] I. J. Ford and R. E. Spinney, Phys. Rev. E **86**, 021127 (2012).
[36] T. Tomé and M. J. de Oliveira, Phys. Rev. Lett. **108**, 020601 (2012).
[37] S. Deffner, Europhys. Lett. **103**, 30001 (2013).
[38] W. Wieczorek, S. G. Hofer, J. Hoelscher-Obermaier, R. Riedinger, K. Hammerer, and M. Aspelmeyer, Phys. Rev. Lett. **114**, 223601 (2015).
[39] D. Nagy, G. Szirmai, and P. Domokos, Phys. Rev. A **84**, 043637 (2011).